nature physics

Article

https://doi.org/10.1038/s41567-024-02436-w

Search for decoherence from quantum gravity with atmospheric neutrinos

Received: 25 July 2023

Accepted: 8 February 2024

Published online: 26 March 2024



Check for updates

The IceCube Collaboration* ⊠

Neutrino oscillations at the highest energies and longest baselines can be used to study the structure of spacetime and test the fundamental principles of quantum mechanics. If the metric of spacetime has a quantum mechanical description, its fluctuations at the Planck scale are expected to introduce non-unitary effects that are inconsistent with the standard unitary time evolution of quantum mechanics. Neutrinos interacting with such fluctuations would lose their quantum coherence, deviating from the expected oscillatory flavour composition at long distances and high energies. Here we use atmospheric neutrinos detected by the IceCube South Pole Neutrino Observatory in the energy range of 0.5–10.0 TeV to search for coherence loss in neutrino propagation. We find no evidence of anomalous neutrino decoherence and determine limits on neutrino-quantum gravity interactions. The constraint on the effective decoherence strength parameter within an energy-independent decoherence model improves on previous limits by a factor of 30. For decoherence effects scaling as E^2 , our limits are advanced by more than six orders of magnitude beyond past measurements compared with the state of the art.

The construction of a consistent and predictive quantum theory of gravity is an outstanding challenge in fundamental physics. A central experimental and theoretical question is whether the metric of spacetime exhibits quantum fluctuations that are intrinsic to all other known fundamental fields. Such fluctuations would represent quantum perturbations in the geometry of spacetime itself, most pronounced on Planck-scale distances or times. At scales below the Planck energy E_P , this sea of spacetime foam¹ could induce small modifications to the standard quantum mechanical time evolution rule of propagating particles, leading to non-unitary effects². The testing for these small violations is one of the few clear experimental avenues through which searches for quantum gravity can be conducted at the single-particle level3.

The oscillations of massive neutrinos between flavour states are a quantum process that has been widely studied over many energies and baselines and with a multitude of neutrino production and detection techniques⁴. Because they interact only through the weak force and gravity, neutrinos are largely isolated from their surroundings and rarely interact as they propagate through matter. This isolation allows quantum coherence to be exhibited over distance scales of thousands of kilometres, enabling neutrino oscillations to serve as a precise interferometer for fundamental studies of the quantum nature of spacetime.

Oscillations of neutrinos produced in cosmic-ray air showers (termed atmospheric neutrinos) have been experimentally verified to maintain quantum coherence over distance scales of at least the diameter of the Earth $(1.2 \times 10^4 \text{ km})^{5.6}$. If propagating neutrinos were to exchange quantum information about their flavour or mass with a fluctuating environment or to experience stochastic perturbations to their quantum phases, their coherence would be lost during travel. Coherence loss causes distinct initial-state wave functions to produce equivalent final states, in violation of quantum mechanical unitarity. Its observation would, therefore, be a smoking-gun signature of neutrinos undergoing quantum gravitational effects that would be difficult to explain by other means³.

The signatures of neutrino decoherence include both a damping of neutrino flavour transitions at large distances and a non-unitary flavour evolution below the oscillation wavelength, which is longer at higher energies. A general description is provided by the formalism of open quantum systems where new superoperators are inserted

^{*}A list of authors and their affiliations appears at the end of the paper. 🖂 e-mail: analysis@icecube.wisc.edu

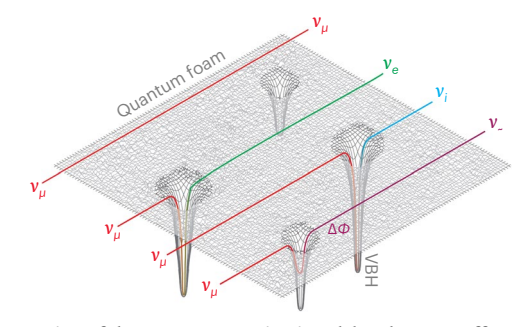


Fig. 1| **Illustration of the quantum gravitational decoherence effect.** Interactions of neutrinos with fluctuating spacetime lead to the decoherence of neutrino oscillations through non-unitary time evolution. In this schematic, the

neutrino oscillations through non-unitary time evolution. In this schematic, the grey grid represents the non-Euclidian background of spacetime foam. The large dips are regions of high curvature, consistent with VBH perturbations. The Roman indices represent mass states; ν_{μ} and $\nu_{e\nu}$, flavour states; and $\nu_{e\nu}$, a phase-perturbed state carrying neither definite mass nor flavour. An incoming neutrino (red) interacting with a VBH may emerge collapsed into a flavour state (green), a mass state (blue) or with its phase perturbed by a random shift $\Delta \phi$ (purple).

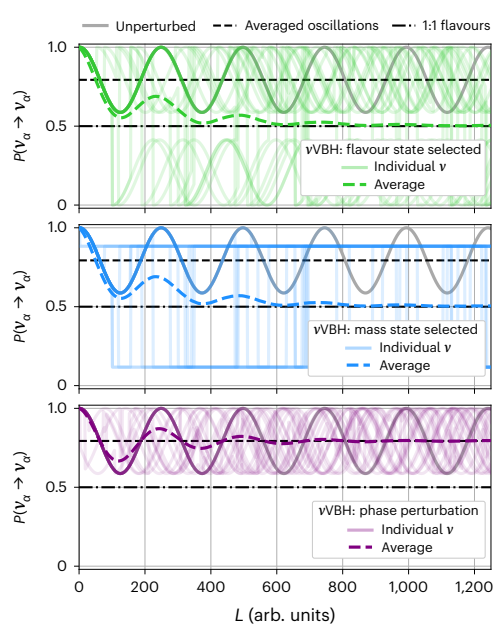


Fig. 2 | **Decoherence of an oscillating neutrino ensemble.** Non-unitary oscillation behaviour can emerge from various types of interaction between neutrinos and VBHs, including absorption with emission in a random-flavour eigenstate (top row), absorption of a neutrino with emission in a random-mass eigenstate (middle row) or a random perturbation to the neutrino phase (bottom row). $P(\nu_{\alpha} \rightarrow \nu_{\alpha})$ represents the survival probability of a neutrino of flavour α over oscillation baseline L, under various vVBH interaction models. The thick solid line represents a non-decohering neutrino, whose amplitude in the wave function is gradually lost as decoherence effects are applied. The semi-transparent lines represent the members of an ensemble of neutrinos stochastically undergoing gravitational perturbations of each type, leading to an ensemble-averaged oscillation probability shown by the dashed lines. The dash–dotted line shows the effect of the complete loss of flavour information for reference. The full phenomenology of these models is described elsewhere 10 .

into the Lindblad master equation⁷. Various mechanisms may give rise to decoherence effects, and their strength, flavour structure and energy dependence may be considered as effective parameters to be interpreted according to a variety of underlying microscopic models. In this work, we will consider two representative flavour structures, where either the neutrino wave function is gradually decohered into

mass or flavour basis states (state selection) or the phase of the neutrino is randomly interrupted (phase perturbation) with equal rates for each neutrino or antineutrino type. Following the original proposal^{8,9}, such effects may be interpreted as emerging from the interaction between propagating particles and virtual black holes (VBHs) generated in quantum fluctuations of the spacetime metric (Fig. 1). When a neutrino is absorbed and re-radiated with its wave function either collapsed or its phase perturbed¹⁰, a stochastic contribution to its time evolution is introduced, leading to coherence loss (Fig. 2). A strikingly similar phenomenology is exhibited in theories^{11,12} in which fluctuations in the metric encode an intrinsic quantum uncertainty into the phase of the particles propagating in otherwise empty spacetime through uncertainty introduced into the time coordinate or path length. Such effects are also observed in models based on a variety of other mechanisms including the deformation of symmetries^{13,14}, metric perturbations^{14,15}, fluctuating minimal lengths^{14,16} and light-cone fluctuations¹⁷. Our results can, therefore, be considered as constraints on a large fraction of potential decoherence scenarios.

Recent searches have been made for vacuum radiation that may be emitted in connection with the decoherence of charged particles 18,19 . Our approach is complementary yet fairly distinct in that (1) neutrinos are electrically neutral, so their collapse would not be expected to produce observable electromagnetic effects; (2) the coherence loss we seek is in the flavour or mass basis rather than in position space; and (3) we directly constrain coherence loss, rather than via the plausible yet speculative interaction between non-unitary collapse processes and an effective acceleration of charges that could generate observable radiation.

Because energy is the cause of spacetime curvature and also because the effects of Planck-scale theories are expected to be suppressed at lower-energy scales, the tests of decoherence emerging from the Planck scale benefit from using the highest possible energies, whereas measurements over the longest possible baselines allow even miniscule effects to accumulate into potentially measurable signals. This makes the IceCube dataset particularly powerful in searching for the signatures of quantum gravitational decoherence. The IceCube Neutrino Observatory²⁰, a neutrino detector within the glacial ice of the Geographic South Pole, occupies 1 km³ of ice from 1,450 to 2,450 m under the surface. A total of 5,160 digital optical modules²¹ are distributed among 86 cables, with a more densely instrumented sub-array called DeepCore²² located at the centre of the detector. IceCube has detected two major populations of high-energy neutrinos: astrophysical neutrinos²³ that dominate the flux of ν_{μ} above 200 TeV and traverse cosmological baselines; and atmospheric neutrinos with a rate peaking at around 1 TeV in IceCube and baselines of up to the diameter of Earth. Although they have the longest baselines and highest energies, searches for decoherence with astrophysical neutrinos^{24,25} are limited by not knowing the oscillation baseline to within an oscillation wavelength, as well as the unknown flavour composition at the source. Although these neutrinos may be used to test for other violations of Lorentz-symmetric quantum mechanical time evolution²⁶, the above considerations inhibit their unambiguous use for decoherence searches. The large ensemble of high-energy atmospheric neutrinos detected by IceCube, however, present an especially compelling window through which to seek evidence of quantum gravitational effects at the single-particle level.

Charged-current interactions of neutrinos with matter produce charged leptons that emit Cherenkov light in identifiable distributions within the detector, which can be categorized into two basic morphologies: tracks and cascades. The electrons from ν_e charged-current interactions yield electromagnetic showers with a roughly spherical distribution of photons (cascade), whereas muons from ν_μ charged-current interactions emit light along a linear trajectory (track). Track events can be further sub-divided into two categories: 'starting tracks' emanating from the detector volume itself and 'through-going tracks' where the neutrino interacted in the ice or rock beneath. The latter category is statistically dominant in this energy

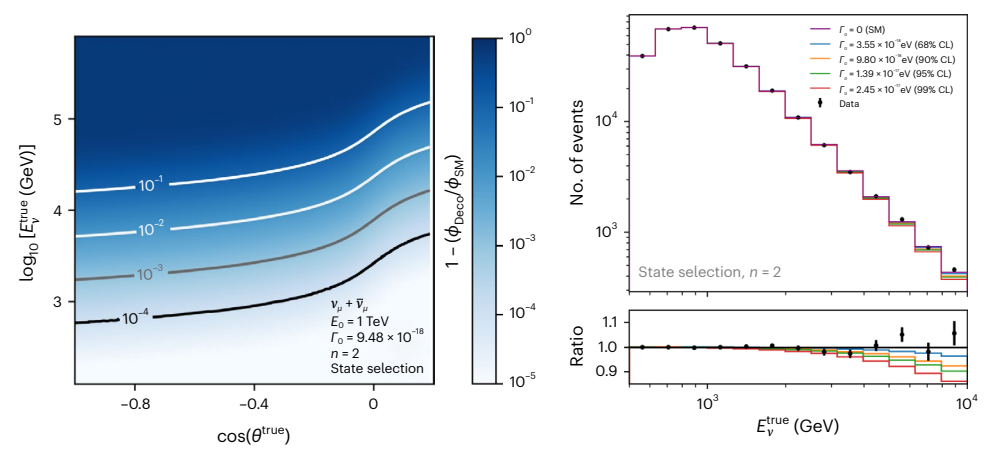


Fig. 3 | **Example neutrino oscillogram and energy spectrum.** Ratio of the predicted v_{μ} flux ϕ_{Deco} for the state selection model with the decoherence parameters listed versus the Standard Model (SM) prediction ϕ_{SM} as a function of the true neutrino energy E_{ν}^{true} and the cosine of true neutrino zenith angle $\cos(\theta^{\text{true}})$ (left). Projection onto true neutrino energy, compared with

approximate statistical precision (right). Γ_0 is the decoherence strength parameter and n, the energy-scaling power-law index about energy pivot point E_0 . The error bars are calculated using Poisson statistics based on the count of data events per bin.

range, due to the much-larger effective target volume. Tau leptons from v_r charged-current interactions have signals with characteristics of both track and cascade morphologies. In addition, neutrinos of all flavours can have neutral-current interactions with matter that produce hadronic showers, in turn inducing cascade signals. This analysis focuses on through-going tracks, which provide a large, high-purity sample of events with which to search for muon–neutrino disappearance signatures induced by decoherence.

Decoherence in neutrino oscillations

Calculating the flavour oscillations of neutrinos detected by IceCube requires the consideration of a plethora of effects, including vacuum oscillations²⁷, coherent forward scattering from matter²⁸, neutrino absorption^{29,30} and τ regeneration^{31,32}. Because the ensemble of neutrinos is subject to both unitary and non-unitary effects (such as absorption and re-interaction), the problem must be approached through the master equation formalism. We perform this calculation using the nuSQuIDS software package³³, by adding decoherence terms to the neutrino oscillation master equation governing the time evolution of the neutrino-reduced density matrix $\rho(t)$. Our parameterization is explained in detail elsewhere¹⁰ and briefly reviewed below.

Atmospheric neutrinos are predominantly produced through the decays of charged pions and kaons³⁴. The production of v_{τ}/\bar{v}_{τ} is highly suppressed, inhibited by the large mass of the τ^{\pm} lepton, which can only be created through the decays of heavy hadrons³⁵. Decoherence effects introduce muon-neutrino disappearance $(v_u \rightarrow v_e)$ and $v_u \rightarrow v_{\tau}$, as well as increased fluxes of v_{τ} at all the energies that exhibit a complex oscillation phenomenology. High-energy v_{τ} undergoing charged-current interactions produce a τ^{\pm} lepton, which weakly decays into a lower-energy v_{τ} as well as produces secondary neutrinos of all the flavours, including additional v_{ij} (refs. 32,36). These secondary neutrinos also oscillate, and lead to further regeneration in the case of the secondary v_r . Because the neutrino flux is a steeply falling function of energy, the disappearance of v_{μ} through decoherence is a substantially larger effect than the appearance of v_{μ} through regeneration from higherenergy v_{τ} , although both are included in our calculations. The small v_{e} contribution to the atmospheric neutrino flux³⁴ is also included in our calculations, although it has only a very minor effect on the oscillation phenomenology. An example oscillogram for a representative set of parameters, showing the change in v_u flux as a function of energy and zenith angle across the high-energy IceCube v_{ij} sample, is shown in Fig. 3 (top). The effect as a function of true neutrino energy alone is shown in Fig. 3 (bottom).

The evolution of a neutrino system with Hamiltonian H and decoherence superoperator $\mathcal{D}[\rho]$ is described (in natural units with $\hbar = c = 1$) as

$$\dot{\rho} = -i[H, \rho] - \mathcal{D}[\rho]. \tag{1}$$

The first term encodes the standard unitary time evolution that drives neutrino oscillations. Our oscillation calculation includes a full description of neutrino mixing and oscillation using the parameters from another work 37 , although the standard neutrino oscillations are negligible in the energy range of this sample. The small uncertainty on decoherence amplitude associated with the neutrino mixing parameters is also irrelevant compared with other sources, and the analysis assumes a normal mass ordering. The second term in equation (1) encapsulates the potentially non-unitary contributions that may be introduced through quantum gravitational effects. A convenient, general form of $\mathcal{D}\left[\rho\right]$ is an expansion in the SU(3) basis $^{10,38-41}$ as

$$\mathcal{D}[\rho] = (D_{\mu\nu}\rho^{\nu})b^{\mu},\tag{2}$$

where ρ^{ν} is the density matrix projection along SU(3) basis vector b^{μ} (the Gell–Mann matrices). $D_{\mu\nu}$ is a 9 × 9 matrix that parameterizes the flavour structure of the decoherence effects on the neutrino system.

In the phase perturbation model (Fig. 2, bottom), the outgoing neutrino state emerges with one or two of the phases of the mass basis states distinctly perturbed. The effect on the average oscillation probability corresponds to a damping that follows:

$$D_{\text{phase perturbation}} = \text{diag}(0, \Gamma, \Gamma, 0, \Gamma, \Gamma, \Gamma, \Gamma, 0), \tag{3}$$

where Γ is the decoherence parameter, with dimensions of energy. At long distances relative to $1/\Gamma$, this model predicts a flux that tends towards an incoherent sum of mass eigenstates. State selection in either the mass or flavour bases impose equivalent overall damping effects, leading to a flux equally weighted in all the neutrino flavours at distances longer than $1/\Gamma$. This democratization is independent of the initial flux and basis of randomization 10 . In the SU(3) basis, the state selection model takes the form

$$D_{\text{state selection}} = \text{diag}(0, \Gamma, \Gamma, \Gamma, \Gamma, \Gamma, \Gamma, \Gamma, \Gamma). \tag{4}$$

Compared with the phase perturbation case, the state selection matrix D has two additional non-zero terms. These are the third and eighth diagonal elements, sometimes referred to as the relaxation terms 42,43 .

The loss of flavour or mass information associated with state selection can be interpreted under a neutrino–virtual black hole (ν VBH) model on the basis of the non-conservation of global quantum numbers by black holes ^{44,45}. This motivates models in which ν emerging from VBH interactions is emitted in states randomly collapsed into a given mass or flavour basis state (Fig. 2, top and middle).

In both models, the neutrino energy E_{ν} dependence of the damping factor Γ is unknown. We, thus, test a representative set of models for $\Gamma(E_{\nu})$, parameterized by

$$\Gamma(E_{\nu}) = \Gamma_0 \left(\frac{E_{\nu}}{E_0}\right)^n,\tag{5}$$

where n is the energy-scaling power, E_0 is an arbitrary reference energy and Γ_0 quantifies the decoherence strength at E_0 . This power-law energy dependence has also been assumed in previous experimental searches for neutrino decoherence 43,46,47 . The values of n and Γ_0 are free parameters, and we take the approach of fixing n and profiling over Γ . Since the curvature of spacetime depends on the energy density, it is natural to expect that the exponent n would be positive. Some models of quantum decoherence due to gravitational effects have suggested an E_{ν}^2 energy scaling $^{48-50}$. The value of Γ_0 for a given model depends on E_0 , which—for convenience—we have set to be close to the peak of the detected neutrino energy distribution at 1 TeV. The value of $\tilde{\Gamma}_0$ for any other choice of \tilde{E}_0 can be obtained via $\Gamma_0 = \tilde{\Gamma}_0 (E_0/\tilde{E}_0)^n$; to compare with past experiments, we present the final results at the reference energy of 1 GeV.

A related quantity is the coherence length $L_{\rm coh}(E)=1/\Gamma(E)$, defined as the distance at which the damping effects resulting from the loss of coherence reach 1/e at a reference neutrino energy. $L_{\rm coh}$ can be interpreted as the ν VBH interaction mean free path 10 , itself dependent on the VBH number density and ν VBH interaction cross section. A natural expectation for decoherence effects emerging from physics at the Planck scale can be obtained by setting $\Gamma(E_P) \geq E_P$. This corresponds to a statement that quantum coherence is effectively impossible at the Planck scale 10,51 . Our results probe deep into this 'Planck-scale naturalness' region of parameter space for energy-scaling factors of $n \lesssim 3$.

Event selection and systematic uncertainties

This Article presents an analysis that constrains decoherence models motivated by quantum gravity with IceCube data using 305,735 reconstructed up-going v_{μ} and \bar{v}_{μ} events in the energy range of 0.5–10.0 TeV. The sample was described in detail in another work⁵², and has been used by the IceCube Collaboration for seeking electronvolt-scale sterile neutrinos through matter-resonant oscillations^{53,54} as well as neutrino–nucleus non-standard interactions⁵⁵.

The event selection provides a sample of track-like events produced by up-going muons traversing the detector. In this energy regime, the tracks tend to be well reconstructed with an energy resolution of $\sigma_{\log_{10}(E_\mu)}\approx 0.3$ and angular resolution $\sigma_{\cos\theta}$ varying between 0.005 and 0.015 as a function of energy. Since cosmic-ray muons are blocked from the up-going flux by the Earth, the event selection is predicted to have a purity of $\gtrsim\!99\%$ of muons generated by charged-current ν_μ interactions below and within the IceCube detector. In scenarios where high-energy ν_τ appearance is enabled (such as decoherence models), the sample also contains a contribution from 17% of leptonic τ decays following ν_τ charged-current interactions below or inside the detector volume.

A detailed discussion of the signal simulation and the suite of systematic uncertainties considered can be found elsewhere ⁵² and is briefly summarized in Extended Data Table 1 and Extended Data Fig. 1. The uncertainty budget includes parameters associated with the primary cosmic-ray flux, hadronic interaction cross sections governing air-shower evolution, the astrophysical neutrino flux, detector performance parameters, ice properties and neutrino interaction cross sections. Each uncertainty contribution is treated as a continuous nuisance

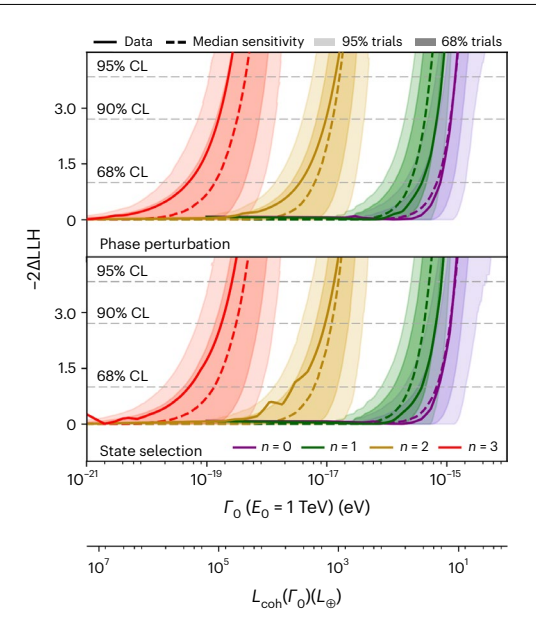


Fig. 4 | **Test statistic distributions.** The 90% CL sensitivity (dashed) and data (solid) analysis test statistic (-2Δ LLH) distributions for phase perturbation (top) and state selection (bottom). Frequentist regions for 95% (darker-shaded region) and 68% (lighter-shaded region) of 1,000 pseudoexperiment trials are also included. The corresponding models of n = 0, 1, 2, 3 are from right to left. Coherence distances L_{coh} at 1 TeV are shown relative to the Earth diameter L_{\oplus} , Γ_0 is the decoherence strength parameter and n is the energy-scaling power-law index about energy pivot point E_0 .

parameter in a likelihood maximization analysis that compares the best-fit likelihood at various values of Γ to establish a unified, frequentist confidence interval for each power index n and decoherence model. The likelihood test statistic follows other work so and is constructed to account for both data and Monte Carlo statistical uncertainties.

We constrain Γ_0 for n=0,1,2,3 using logarithmically binned events in reconstructed muon energy $\log(E^\mu_{\rm reco})$ (13 bins, $E^\mu_{\rm reco} \in [500, 9,976]$ GeV) and uniformly in zenith angle (20 bins, $\cos(\theta^\mu_{\rm reco}) \in [-1.0,0]$). This constraint is evaluated under the two aforementioned flavour structures, although since our sample predominantly comprises tracks produced by ν_μ and $\bar{\nu}_\mu$ interactions, it is relatively insensitive to the detailed flavour structure of the decoherence operators so long as ν_μ decoherence is present.

Constraints on anomalous decoherence

The analysis was blindly developed using simulated data and then applied to real data following a staged unblinding protocol developed for IceCube oscillation measurements. Before unblinding, the median analysis sensitivity in the event of a null signal and its 68% and 95% envelopes were established using 1,000 Monte Carlo pseudoexperiments. The expected analysis performance in the event of an injected signal was also tested. Signals beyond the 90% contour were exactly recovered in un-fluctuated fits and with the expected level of accuracy when data fluctuations were included.

A multistage blind-fit procedure was followed, first checking the energy and zenith pull distributions and then one-dimensional histograms at the best-fit point, followed by nuisance parameter pulls, the joint [energy, zenith] distribution and pulls and finally unblinding the full result. Extended Data Table 1 and Extended Data Fig. 1 provide a list of the best-fit values and pulls of all the systematic uncertainty parameters. The result is consistent with the null hypothesis for all the decoherence models. The *P* value, defined as the fraction of simulated decoherence-free pseudoexperiments with test statistic larger than that observed in the data, is in the range of 0.59–0.61 for each tested decoherence model and energy-scaling

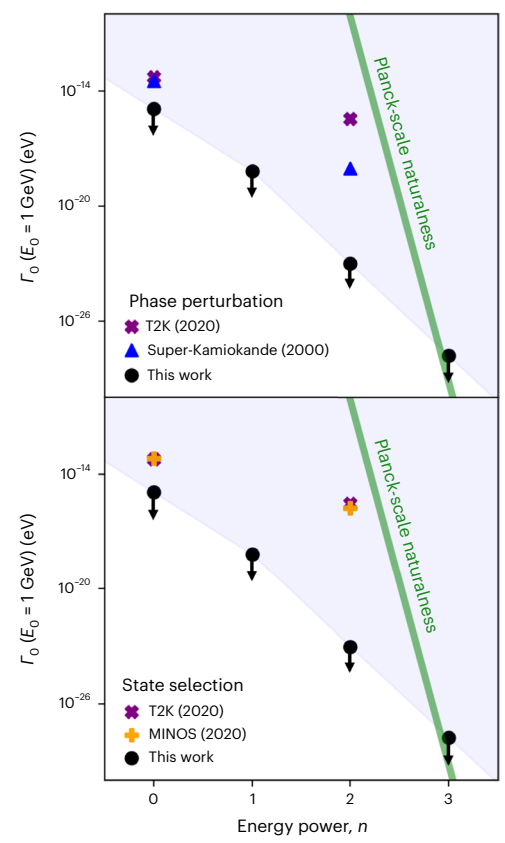


Fig. 5 | **Comparison with previous results.** Comparison of limits from both analyses on the phase perturbation interaction model to previous results (top). Comparison of limits from both analyses on the state selection interaction model to previous results (bottom). Γ_0 is the decoherence strength parameter and n is the energy-scaling power-law index about energy pivot point E_0 . The blue triangles represent results from Super-Kamiokande⁴⁶ and orange + markers and purple × markers represent results from MINOS and T2K, respectively, as derived from another work⁴³. The green lines indicate the expected size of decoherence parameter for effects originating at the Planck scale and follow a single power law to observable scales. The black data points are the results of this analysis, with the arrows pointing into the allowed region, and shading representing the excluded region on the basis of this analysis.

power n. The final upper limits on the decoherence parameter Γ in all the cases fall within the 68% envelope of values expected if no decoherence is present (Fig. 4). Feldman–Cousins ensemble tests were performed at the 90% confidence level (CL) positions to check for proper coverage ⁵⁷. The 90% CL locations from Wilks' theorem were found to be slightly weaker than the Feldman–Cousins values, with the maximum deviation of 28.2% in the value of Γ at 90.0% CL. This difference is imperceptible on the logarithmic Γ axes (Figs. 4 and 5). The 90% confidence limits from this analysis Γ_{90} (E_0 = 1 TeV) for the state selection and phase perturbation scenarios are tabulated in Table 1. For reference, Fig. 4 also lists the corresponding coherence lengths for a 1 TeV neutrino.

We, thus, report strong constraints on the magnitude of anomalous decoherence from quantum gravity as neutrinos oscillate across the Earth. Using flavour structures motivated by neutrino interactions with spacetime foam having four power-law models and two representative flavour structures, 90% CL limits have been obtained on the parameter Γ_0 with pivot energy $E_0 = 1$ TeV. To facilitate comparison with previous studies, our results can be mapped to the pivot energy of 1 GeV that has tended to be favoured by previous works. A comparison with past data is shown in Fig. 5. For all the tested power-law indices and both tested flavour models, the results presented in this paper provide the

Table 1 | Summary of constraints on decoherence models obtained in this analysis

n	Phase perturbation Γ_{90}	State selection Γ_{90}
0	1.18×10 ⁻¹⁵ eV	1.17×10 ⁻¹⁵ eV
1	6.89×10 ⁻¹⁶ eV	6.67×10 ⁻¹⁶ eV
2	9.80×10 ⁻¹⁸ eV	9.48×10 ⁻¹⁸ eV
3	1.58×10 ⁻¹⁹ eV	1.77×10 ⁻¹⁹ eV

The 90% CL upper limits on decoherence strength parameter Γ_0 (which we name Γ_{90}) are reported for each power-law index n with power-law pivot energy E_0 =1TeV in the state selection and phase perturbation models.

world's strongest limits. In all the cases with n < 3, the limits significantly surpass the natural Planck-scale benchmark.

The energy-independent (n=0) scenario has been explored previously for T2K⁴³, Super-Kamiokande⁴⁶ and MINOS⁴³. The IceCube limits extend beyond the past measurements by a factor of around 30 for the state selection model and 50 for phase perturbations, owing to the larger sample size of the IceCube atmospheric neutrino dataset.

The substantially increased energy range of the IceCube atmospheric neutrino sample leads to a far more dramatic improvement in sensitivity for models where the decoherence strength depends on energy with a positive exponent. Past results have been obtained for the gravity-motivated n=2 model^{48–50} by the aforementioned three experiments, which primarily collect neutrinos at around three orders of magnitude lower energy than the peak of the IceCube sample. We report improvements by six orders of magnitude in the phase perturbation model and eight orders of magnitude in the state selection model. Since quantum gravitational effects are anticipated to positively scale with energy density, the limits presented in this paper represent a major increase in sensitivity to anomalous decoherence from quantum gravity in the neutrino sector.

Online content

Any methods, additional references, Nature Portfolio reporting summaries, source data, extended data, supplementary information, acknowledgements, peer review information; details of author contributions and competing interests; and statements of data and code availability are available at https://doi.org/10.1038/s41567-024-02436-w.

References

- 1. Wheeler, J. A. Geons. *Phys. Rev.* **97**, 511–536 (1955).
- Carlip, S. Spacetime foam: a review. Rep. Progr. Phys. 86, 066001 (2023).
- Carney, D., Stamp, P. C. & Taylor, J. M. Tabletop experiments for quantum gravity: a user's manual. Class. Quantum Grav. 36, 034001 (2019).
- Tanabashi, M. et al. Review of particle physics: particle data groups. Phys. Rev. D 98, 030001 (2018).
- Jung, C. K., McGrew, C., Kajita, T. & Mann, T. Oscillations of atmospheric neutrinos. *Annu. Rev. Nucl. Part. Sci.* 51, 451–488 (2001).
- Gaisser, T. K. & Honda, M. Flux of atmospheric neutrinos. Annu. Rev. Nucl. Part. Sci. 52, 153–199 (2002).
- Schlosshauer, M. Decoherence and the Quantum-to-Classical Transition (Springer, 2007).
- Hawking, S. W. Virtual black holes. Phys. Rev. D 53, 3099–3107 (1996).
- 9. 't Hooft, G. Virtual black holes and space-time structure. *Found. Phys.* **48**, 1134–1149 (2018).
- Stuttard, T. & Jensen, M. Neutrino decoherence from quantum gravitational stochastic perturbations. *Phys. Rev. D* 102, 115003 (2020).

- Penrose, R. On gravity's role in quantum state reduction. Gen. Relat. Gravit. 28, 581–600 (1996).
- 12. Diosi, L. A universal master equation for the gravitational violation of quantum mechanics. *Phys. Lett. A* **120**, 377–381 (1987).
- 13. Arzano, M., D'Esposito, V. & Gubitosi, G. Fundamental decoherence from quantum spacetime. *Commun. Phys.* **6**, 242 (2023).
- 14. D'Esposito, V. & Gubitosi, G. Constraints on quantum spacetime-induced decoherence from neutrino oscillations. Preprint at https://arxiv.org/abs/2306.14778 (2023).
- Goklu, E., Lammerzahl, C. & Breuer, H.-P. Metric fluctuations and decoherence. In 12th Marcel Grossmann Meeting on General Relativity 2420–2422 (2009).
- Petruzziello, L. & Illuminati, F. Quantum gravitational decoherence from fluctuating minimal length and deformation parameter at the Planck scale. Nat. Commun. 12, 4449 (2021).
- Stuttard, T. Neutrino signals of lightcone fluctuations resulting from fluctuating spacetime. Phys. Rev. D 104, 056007 (2021).
- Donadi, S. et al. Underground test of gravity-related wave function collapse. Nat. Phys. 17, 74–78 (2021).
- Arnquist, I. et al. Search for spontaneous radiation from wave function collapse in the Majorana demonstrator. *Phys. Rev. Lett.* 129, 080401 (2022).
- Aartsen, M. G. et al. The IceCube neutrino observatory: instrumentation and online systems. JINST 12, 03012 (2017).
- Abbasi, R. et al. The IceCube data acquisition system: signal capture, digitization, and timestamping. *Nucl. Instrum. Methods Phys. Res.*, Sect. A 601, 294–316 (2009).
- 22. Abbasi, R. et al. The design and performance of IceCube DeepCore. *Astropart. Phys.* **35**, 615–624 (2012).
- 23. Aartsen, M. G. Observation of high-energy astrophysical neutrinos in three years of IceCube data. *Phys. Rev. Lett.* **113**, 101101 (2014).
- Christian, J. Testing gravity-driven collapse of the wave function via cosmogenic neutrinos. *Phys. Rev. Lett.* 95, 160403 (2005).
- Hellmann, D., Päs, H. & Rani, E. Searching new particles at neutrino telescopes with quantum-gravitational decoherence. *Phys. Rev. D* 105, 055007 (2022).
- Aartsen, M. G. et al. Neutrino interferometry for high-precision tests of Lorentz symmetry with IceCube. *Nat. Phys.* 14, 961–966 (2018).
- 27. Giunti, C. & Kim, C. W. Fundamentals of Neutrino Physics and Astrophysics (Oxford Univ. Press. 2007).
- Mikheev, S. P. & Smirnov, A. Y. Resonance oscillations of neutrinos in matter. Sov. Phys. Usp. 30, 759–790 (1987).
- 29. Cooper-Sarkar, A., Mertsch, P. & Sarkar, S. The high energy neutrino cross-section in the Standard Model and its uncertainty. *J. High Energ. Phys.* **2011**, 042 (2011).
- IceCube Collaboration. Measurement of the multi-TeV neutrino interaction cross-section with icecube using Earth absorption. Nature 551, 596–600 (2017).
- Beacom, J. F., Crotty, P. & Kolb, E. W. Enhanced signal of astrophysical tau neutrinos propagating through Earth. *Phys. Rev.* D 66, 021302 (2002).
- 32. Argüelles, C. A., Garg, D., Patel, S., Reno, M. H. & Safa, I. Tau depolarization at very high energies for neutrino telescopes. *Phys. Rev. D* **106**, 043008 (2022).
- Argüelles, C. A., Salvado, J. & Weaver, C. N. nuSQuIDS: a toolbox for neutrino propagation. Comput. Phys. Commun. 277, 108346 (2022).
- 34. Fedynitch, A., Engel, R., Gaisser, T. K., Riehn, F. & Stanev, T. Calculation of conventional and prompt lepton fluxes at very high energy. *EPJ Web Conf.* **99**, 08001 (2015).
- Bhattacharya, A., Enberg, R., Reno, M. H., Sarcevic, I. & Stasto, A. Perturbative charm production and the prompt atmospheric neutrino flux in light of RHIC and LHC. J. High Energ. Phys. 06, 110 (2015).

- Safa, I. et al. TauRunner: a public Python program to propagate neutral and charged leptons. Comput. Phys. Commun. 278, 108422 (2022).
- Esteban, I., Gonzalez-Garcia, M., Maltoni, M., Martinez-Soler, I. & Schwetz, T. Updated fit to three neutrino mixing: exploring the accelerator-reactor complementarity. J. High Energ. Phys. 2017, 087 (2017).
- Gago, A. M., Santos, E. M., Teves, W. J. C. & Zukanovich Funchal, R. A study on quantum decoherence phenomena with three generations of neutrinos. Preprint at https://arxiv.org/abs/ hep-ph/0208166 (2002).
- 39. Benatti, F. & Floreanini, R. Open system approach to neutrino oscillations. *J. High Energ. Phys.* **02**, 032 (2000).
- Carrasco, J. C., Díaz, F. N. & Gago, A. M. Probing CPT breaking induced by quantum decoherence at DUNE. *Phys. Rev. D* 99, 075022 (2019).
- Buoninfante, L., Capolupo, A., Giampaolo, S. M. & Lambiase, G. Revealing neutrino nature and CPT violation with decoherence effects. Eur. Phys. J. C 80, 1009 (2020).
- 42. Guzzo, M. M., de Holanda, P. C. & Oliveira, R. L. N. Quantum dissipation in a neutrino system propagating in vacuum and in matter. *Nucl. Phys. B* **908**, 408–422 (2016).
- 43. Gomes, A. L. G., Gomes, R. A. & Peres, O. L. G. Quantum decoherence and relaxation in long-baseline neutrino data. *J. High Energ. Phys.* **2023**, 35 (2023).
- 44. Anchordoqui, L. A. et al. Probing Planck scale physics with IceCube. *Phys. Rev. D* 72, 065019 (2005).
- 45. Klapdor-Kleingrothaus, H., Päs, H. & Sarkar, U. Effects of quantum space time foam in the neutrino sector. *Eur. Phys. J. A* **8**, 577–580 (2000).
- Lisi, E., Marrone, A. & Montanino, D. Probing possible decoherence effects in atmospheric neutrino oscillations. *Phys. Rev. Lett.* 85, 1166–1169 (2000).
- Coloma, P., Lopez-Pavon, J., Martinez-Soler, I. & Nunokawa, H. Decoherence in neutrino propagation through matter, and bounds from IceCube/DeepCore. *Eur. Phys. J. C* 78, 614 (2018).
- Ellis, J., Mavromatos, N. & Nanopoulos, D. Quantum decoherence in a D-foam background. *Mod. Phys. Lett. A* 12, 1759–1773 (1997).
- Ellis, J. R., Mavromatos, N. E., Nanopoulos, D. V. & Winstanley, E. Quantum decoherence in a four-dimensional black hole background. *Mod. Phys. Lett. A* 12, 243–256 (1997).
- 50. Benatti, F. & Floreanini, R. Non-standard neutral kaon dynamics from infinite statistics. *Ann. Phys.* **273**, 58–71 (1999).
- Adams, F. C., Kane, G. L., Mbonye, M. & Perry, M. J. Proton decay, black holes, and large extra dimensions. *Int. J. Mod. Phys. A* 16, 2399–2410 (2001).
- Aartsen, M. G. et al. Searching for eV-scale sterile neutrinos with eight years of atmospheric neutrinos at the IceCube Neutrino Telescope. *Phys. Rev. D* 102, 052009 (2020).
- Aartsen, M. G. et al. eV-scale sterile neutrino search using eight years of atmospheric muon neutrino data from the IceCube Neutrino Observatory. *Phys. Rev. Lett.* 125, 141801 (2020).
- Abbasi, R. et al. Search for unstable sterile neutrinos with the IceCube Neutrino Observatory. *Phys. Rev. Lett.* 129, 151801 (2022).
- Abbasi, R. et al. Strong constraints on neutrino nonstandard interactions from TeV-scale v_u disappearance at IceCube. *Phys. Rev. Lett.* 129, 011804 (2022).
- 56. Argüelles, C. A., Schneider, A. & Yuan, T. A binned likelihood for stochastic models. *J. High Energ. Phys.* **06**, 030 (2019).
- Feldman, G. J. & Cousins, R. D. A unified approach to the classical statistical analysis of small signals. *Phys. Rev. D* 57, 3873–3889 (1998).

Publisher's note Springer Nature remains neutral with regard to jurisdictional claims in published maps and institutional affiliations.

Springer Nature or its licensor (e.g. a society or other partner) holds exclusive rights to this article under a publishing agreement with

the author(s) or other rightsholder(s); author self-archiving of the accepted manuscript version of this article is solely governed by the terms of such publishing agreement and applicable law.

© The Author(s), under exclusive licence to Springer Nature Limited 2024

The IceCube Collaboration

R. Abbasi¹, M. Ackermann², J. Adams³, S. K. Agarwalla^{4,65}, J. A. Aguilar⁵, M. Ahlers⁶, J. M. Alameddine⁷, N. M. Amin⁸, K. Andeen⁹, G. Anton¹⁰, C. Argüelles¹¹, Y. Ashida¹², S. Athanasiadou², L. Ausborm¹³, S. N. Axani⁸, X. Bai¹⁴, A. Balagopal V⁴, M. Baricevic⁴, S. W. Barwick¹⁵, V. Basu⁴, R. Bay¹⁶, J. J. Beatty^{17,18}, J. Becker Tjus^{19,66}, J. Beise²⁰, C. Bellenghi²¹, C. Benning¹³, S. BenZvi²², D. Berley²³, E. Bernardini²⁴, D. Z. Besson²⁵, E. Blaufuss²³, S. Blot², F. Bontempo²⁶, J. Y. Book¹¹, C. Boscolo Meneguolo²⁴, S. Böser²⁷, O. Botner²⁰, J. Böttcher¹³, J. Braun⁴, B. Brinson²⁸, J. Brostean-Kaiser², L. Brusa¹³, R. T. Burley²⁹, R. S. Busse³⁰, D. Butterfield⁴, M. A. Campana³¹. K. Carloni¹¹, E. G. Carnie-Bronca²⁹, S. Chattopadhyay^{4,65}, N. Chau⁵, C. Chen²⁸, Z. Chen³², D. Chirkin⁴, S. Choi³³, B. A. Clark²³, A. Coleman²⁰, G. H. Collin³⁴, A. Connolly^{17,18}, J. M. Conrad³⁴, P. Coppin³⁵, P. Correa³⁵, D. F. Cowen^{36,37}, P. Dave²⁸, C. De Clercq³⁵, J.J. DeLaunay³⁸, D. Delgado¹¹, S. Deng¹³, K. Deoskar³⁹, A. Desai⁴, P. Desiati⁴, K. D. de Vries³⁵, G. de Wasseige⁴⁰, T. DeYoung⁴¹, A. Diaz³⁴, J. C. Díaz-Vélez⁴, M. Dittmer³⁰, A. Domi¹⁰, H. Dujmovic⁴, M. A. DuVernois⁴, T. Ehrhardt²⁷, A. Eimer¹⁰, P. Eller²¹, E. Ellinger⁴², S. El Mentawi¹³, D. Elsässer⁷, R. Engel^{26,43}, H. Erpenbeck⁴, J. Evans²³, P. A. Evenson⁸, K. L. Fan²³, K. Fanrag⁴⁴, A. R. Fazely⁴⁵, A. Fedynitch⁴⁶, N. Feigl⁴⁷, S. Fiedlschuster¹⁰, C. Finley³⁹, L. Fischer², D. Fox³⁶, A. Franckowiak¹⁹, P. Fürst¹³, J. Gallagher⁴⁸, E. Ganster¹³, A. Garcia¹¹, L. Gerhardt⁴⁹, A. Ghadimi³⁸, C. Glaser²⁰, T. Glüsenkamp^{10,20}, J. G. Gonzalez⁸, D. Grant⁴¹, S. J. Gray²³, O. Gries¹³, S. Griffin⁴, S. Griswold²², K. M. Groth⁶, C. Günther¹³, P. Gutjahr⁷, C. Ha⁵⁰, C. Haack¹⁰, A. Hallgren²⁰, R. Halliday⁴¹, L. Halve¹³, F. Halzen⁴, H. Hamdaoui³², M. Ha Minh²¹, M. Handt¹³, K. Hanson⁴, J. Hardin³⁴, A. A. Harnisch⁴¹, P. Hatch⁵¹, A. Haungs²⁶, J. Häußler¹³, H. Hamdaoui³⁻, M. Ha Minn⁴⁻, M. Handt³, K. Hanson⁴, J. Hardin³, A. A. Harnisch³, P. Hatch³, A. Haungs³⁻, J. Haungs³⁻, J. Haungs³⁻, J. Hellrung¹⁹, J. Hermannsgabner¹³, L. Heuermann¹³, N. Heyer²⁰, S. Hickford⁴², A. Hidvegi³⁹, C. Hill⁴⁴, G. C. Hill²⁹, K. D. Hoffman²³, S. Hori⁴, K. Hoshina^{4,67}, W. Hou²⁶, T. Huber²⁶, K. Hultqvist³⁹, M. Hünnefeld⁷, R. Hussain⁴, K. Hymon⁷, S. In³³, A. Ishihara⁴⁴, M. Jacquart⁴, O. Janik¹³, M. Jansson³⁹, G. S. Japaridze⁵², M. Jeong¹², M. Jin¹¹, B. J. P. Jones⁵³, N. Kamp¹¹, D. Kang²⁶, W. Kang³³, X. Kang³¹, A. Kappes³⁰, D. Kappesser²⁷, L. Kardum⁷, T. Karg², M. Karl²¹, A. Karle⁴, A. Katil⁵⁴, U. Katz¹⁰, M. Kauer⁴, J. L. Kelley⁴, A. Khatee Zathul⁴, A. Kheirandish^{55,56}, J. Kiryluk³², S. R. Klein^{16,49}, A. Kochocki⁴¹, R. Koirala⁸, H. Kolanoski⁴⁷, T. Kontrimas²¹, L. Köpke²⁷, C. Kopper¹⁰, D. J. Koskinen⁶, P. Koundal²⁶, M. Kovacevich³¹, M. Kowalski^{2,47}, T. Kozynets⁶, J. Krishnamoorthi^{4,65}, K. Kruiswijk⁴⁰, E. Krupczak⁴¹, A. Kumar², E. Kun¹⁹, N. Kurahashi³¹, N. Lad², C. Lagunas Gualda², M. Lamoureux⁴⁰, M. J. Larson²³, S. Latseva¹³, F. Lauber⁴², J. P. Lazar^{4,11}, J. W. Lee³³, K. Leonard DeHolton³⁷, A. Leszczyńska⁸, M. Lincetto¹⁹, Y. Liu^{36,37}, M. Liubarska⁵⁴, E. Lohfink²⁷, C. Love³¹, C. J. Lozano Mariscal³⁰, L. Lu⁴, F. Lucarelli⁵⁷, W. Luszczak^{17,18}, Y. Lyu^{16,49}, J. Madsen⁴, E. Magnus³⁵, K. B. M. Mahn⁴¹, Y. Makino⁴, E. Manao²¹, S. Mancina^{4,24}, W. Marie Sainte⁴, I. C. Mariş⁵, S. Marka⁵⁸, Z. Marka⁵⁸, M. Marsee³⁸, I. Martinez-Soler¹¹, R. Maruyama⁵⁹, F. Mayhew⁴¹, T. McElroy⁵⁴, F. McNally⁶⁰, J. V. Mead⁶, K. Meagher⁴, S. Mechbal², A. Medina¹⁸, M. Meier⁴⁴, Y. Merckx³⁵, L. Merten¹⁹, J. Micallef⁴¹, J. Mitchell⁴⁵, T. Montaruli⁵⁷, R. W. Moore⁵⁴, Y. Morii⁴⁴, R. Morse⁴, M. Moulai⁴, T. Mukherjee²⁶, R. Naab², R. Nagai⁴⁴, M. Nakos⁴, U. Naumann⁴², J. Necker², A. Negi⁵³, M. Neumann³⁰, H. Niederhausen⁴¹, M. U. Nisa⁴¹, A. Noell¹³, A. Novikov⁸, S. C. Nowicki⁴¹, A. Obertacke Pollmann⁴⁴, V. O'Dell⁴, B. Oeyen⁶¹, A. Olivas²³, R. Orsoe²¹, J. Osborn⁴, E. O'Sullivan²⁰, H. Pandya⁸, N. Park⁵¹, G. K. Parker⁵³, E. N. Paudel⁸, L. Paul¹⁴, C. Pérez de los Heros²⁰, T. Pernice², I. Peterson⁴, S. Philippen¹³, A. Pizzuto⁴, M. Plum¹⁴, A. Pontén²⁰, Y. Popovych²⁷, M. Prado Rodriguez⁴, B. Pries⁴¹, R. Procter-Murphy²³, G. T. Przybylski⁴⁹, C. Raab⁴⁰, J. Rack-Helleis²⁷, K. Rawlins⁶², Z. Rechav⁴, A. Rehman⁸, P. Reichherzer¹⁹, E. Resconi²¹, S. Reusch², W. Rhode⁷, B. Riedel⁴, A. Rifaie¹³, E. J. Roberts²⁹, S. Robertson^{16,49}, S. Rodan³³, G. Roellinghoff³³, M. Rongen¹⁰, A. Rosted⁴⁴, C. Rott^{12,33}, T. Ruhe⁷, L. Ruohan²¹, D. Ryckbosch⁶¹, I. Safa^{4,11}, J. Saffer⁴³, D. Salazar-Gallegos⁴¹, P. Sampathkumar²⁶, S. E. Sanchez Herrera⁴¹, A. Sandrock⁴², M. Santander³⁸, S. Sarkar⁵⁴, S. Sarkar⁶³, J. Savelberg¹³, P. Savina⁴, M. Schaufel¹³, H. Schieler²⁶, S. Schindler¹⁰, L. Schlickmann¹³, B. Schlüter³⁰, F. Schlüter⁵, N. Schmeisser⁴², T. Schmidt²³, J. Schneider¹⁰, F. G. Schröder^{8,26}, L. Schumacher¹⁰, S. Sclafani²³, D. Seckel⁸, M. Seikh²⁵, S. Seunarine⁶⁴, R. Shah³¹, S. Shefali⁴³, N. Shimizu⁴⁴, M. Silva⁴, B. Skrzypek¹¹, B. Smithers⁵³, R. Snihur⁴, J. Soedingrekso⁷, A. Søgaard⁶, D. Soldin⁴³, P. Soldin¹³, G. Sommani¹⁹, C. Spannfellner²¹, G. M. Spiczak⁶⁴, C. Spiering², M. Stamatikos¹⁸, T. Stanev⁸, T. Stezelberger⁴⁹, T. Stürwald⁴², T. Stuttard⁶, G. W. Sullivan²³, I. Taboada²⁸, S. Ter-Antonyan⁴⁵, A. Terliuk²¹, M. Thiesmeyer¹³, W. G. Thompson¹¹, J. Thwaites⁴, S. Tilav⁸, K. Tollefson⁴¹, C. Tönnis³³, S. Toscano⁵, D. Tosi⁴, A. Trettin², C. F. Tung²⁸, R. Turcotte²⁶, J. P. Twagirayezu⁴¹, M. A. Unland Elorrieta³⁰, A. K. Upadhyay^{4,65}, K. Upshaw⁴⁵, A. Vaidyanathan⁹, N. Valtonen-Mattila²⁰, J. Vandenbroucke⁴, N. van Eijndhoven³⁵, D. Vannerom³⁴, J. van Santen², J. Vara³⁰, J. Veitch-Michaelis⁴, M. Venugopal²⁶, M. Vereecken⁴⁰, S. Verpoest⁸, D. Veske⁵⁸, A. Vijai²³, C. Walck³⁹, Y. Wang^{36,37}, C. Weaver⁴¹, P. Weigel³⁴, A. Weindl²⁶, J. Weldert³⁷, A. Y. Wen¹¹, C. Wendt⁴, J. Werthebach⁷, M. Weyrauch²⁶, N. Whitehorn⁴¹, C. H. Wiebusch¹³, D. R. Williams³⁸, L. Williams³⁸, A. Wolf¹³, M. Wolf²¹, G. Wrede¹⁰, Werthelbach⁷, M. Weyrauch²⁶, N. Whitehorn⁴¹, C. H. Wiebusch¹³, D. R. Williams³⁸, L. Williams³⁸, A. Wolf¹³, M. Wolf²¹, G. Wrede¹⁰, Western⁴, C. X. W. Xu⁴⁵, J. P. Yanez⁵⁴, E. Yildizci⁴, S. Yoshida⁴⁴, R. Young²⁵, S. Yu⁴¹, T. Yuan⁴, Z. Zhang³², P. Zhelnin¹¹, P. Zilberman⁴ & M. Zimmerman4

¹Department of Physics, Loyola University Chicago, Chicago, IL, USA. ²Deutsches Elektronen-Synchrotron DESY, Zeuthen, Germany. ³Department of Physics and Astronomy, University of Canterbury, Christchurch, New Zealand. ⁴Department of Physics and Wisconsin IceCube Particle Astrophysics Center, University of Wisconsin-Madison, Madison, WI, USA. ⁵Université Libre de Bruxelles, Science Faculty, Brussels, Belgium. ⁶Niels Bohr Institute, University of Copenhagen, Copenhagen, Denmark. ⁷Department of Physics, TU Dortmund University, Dortmund, Germany. ⁸Bartol Research Institute and Department of Physics and Astronomy, University of Delaware, Newark, DE, USA. ⁹Department of Physics, Marquette University, Milwaukee, WI, USA. ¹⁰Erlangen Centre for Astroparticle Physics, Friedrich-Alexander-Universität Erlangen-Nürnberg, Erlangen, Germany. ¹¹Department of Physics and Laboratory for Particle Physics and Cosmology, Harvard University, Cambridge, MA, USA. ¹²Department of Physics and Astronomy, University of

Utah, Salt Lake City, UT, USA. 13 III. Physikalisches Institut, RWTH Aachen University, Aachen, Germany. 14 Physics Department, South Dakota School of Mines and Technology, Rapid City, SD, USA, 15 Department of Physics and Astronomy, University of California, Irvine, CA, USA, 16 Department of Physics, University of California, Berkeley, CA, USA. ¹⁷Department of Astronomy, Ohio State University, Columbus, OH, USA. ¹⁸Department of Physics and Center for Cosmology and Astro-Particle Physics, Ohio State University, Columbus, OH, USA. 19 Fakultät für Physik & Astronomie, Ruhr-Universität Bochum, Bochum, Germany. 20 Department of Physics and Astronomy, Uppsala University, Uppsala, Sweden. 21 Physik-department, Technische Universität München, Garching, Germany. 22 Department of Physics and Astronomy, University of Rochester, Rochester, NY, USA. 23 Department of Physics, University of Maryland, College Park, MD, USA. 24Dipartimento di Fisica e Astronomia Galileo Galilei, Università Degli Studi di Padova, Padova, Italy. 25Department of Physics and Astronomy, University of Kansas, Lawrence, KS, USA. 26 Karlsruhe Institute of Technology, Institute for Astroparticle Physics, Karlsruhe, Germany. 27 Institute of Physics, University of Mainz, Mainz, Germany. 28 School of Physics and Center for Relativistic Astrophysics, Georgia Institute of Technology, Atlanta, GA, USA. 29 Department of Physics, University of Adelaide, Adelaide, South Australia, Australia. 30 Institut für Kernphysik, Westfälische Wilhelms-Universität Münster, Münster, Germany. 31 Department of Physics, Drexel University, Philadelphia, PA, USA. 32 Department of Physics and Astronomy, Stony Brook University, Stony Brook, NY, USA. 33 Department of Physics, Sungkyunkwan University, Suwon, Republic of Korea. 44 Department of Physics, Massachusetts Institute of Technology, Cambridge, MA, USA. 35 Vrije Universiteit Brussel (VUB), Dienst ELEM, Brussels, Belgium. 36 Department of Astronomy and Astrophysics, Pennsylvania State University, University Park, PA, USA, 37Department of Physics, Pennsylvania State University, University Park, PA, USA. 38 Department of Physics and Astronomy, University of Alabama, Tuscaloosa, AL, USA. 39 Oskar Klein Centre and Department of Physics, Stockholm University, Stockholm, Sweden. 40Centre for Cosmology, Particle Physics and Phenomenology—CP3, Université catholique de Louvain, Louvain-la-Neuve, Belgium. 41Department of Physics and Astronomy, Michigan State University, East Lansing, MI, USA. 42Department of Physics, University of Wuppertal, Wuppertal, Germany. 43 Karlsruhe Institute of Technology, Institute of Experimental Particle Physics, Karlsruhe, Germany. 44 Department of Physics and The International Center for Hadron Astrophysics, Chiba University, Chiba, Japan. 45 Department of Physics, Southern University, Baton Rouge, LA, USA. 46 Institute of Physics, Academia Sinica, Taipei, Taiwan. 47 Institut für Physik, Humboldt-Universität zu Berlin, Berlin, Germany. 48 Department of Astronomy, University of Wisconsin-Madison, Madison, WI, USA. 49 Lawrence Berkeley National Laboratory, Berkeley, CA, USA. 50 Department of Physics, Chung-Ang University, Seoul, Korea. 51Department of Physics, Engineering Physics, and Astronomy, Queen's University, Kingston, Ontario, Canada. ⁵²CTSPS, Clark-Atlanta University, Atlanta, GA, USA. ⁵³Department of Physics, University of Texas at Arlington, Arlington, TX, USA. ⁵⁴Department of Physics, University of Alberta, Edmonton, Alberta, Canada. 55Department of Physics & Astronomy, University of Nevada, Las Vegas, NV, USA. 56Nevada Center for Astrophysics, University of Nevada, Las Vegas, NV, USA. 57 Département de physique nucléaire et corpusculaire, Université de Genève, Genève, Switzerland. 58 Columbia Astrophysics and Nevis Laboratories, Columbia University, New York, NY, USA. 59 Department of Physics, Yale University, New Haven, CT, USA. 60 Department of Physics, Mercer University, Macon, GA, USA. 61 Department of Physics and Astronomy, University of Gent, Gent, Belgium. 62Department of Physics and Astronomy, University of Alaska Anchorage, Anchorage, AK, USA. 63Department of Physics, University of Oxford, Oxford, UK. 64Department of Physics, University of Wisconsin, River Falls, WI, USA. 65 Present address: Institute of Physics, Sachivalaya Marg, Sainik School Post, Bhubaneswar, India. 66 Present address: Department of Space, Earth and Environment, Chalmers University of Technology, Gothenburg, Sweden. ⁶⁷Present address: Earthquake Research Institute, University of Tokyo, Bunkyo, Japan.

Methods

Simulation methods and systematic uncertainties

To predict the expected rate of up-going tracks selected as a function of zenith and energy, a three-flavour prediction of neutrino flux emerging from cosmic-ray air showers is first made using the MCEq software package³⁴.

The simulation of neutrino flux with MCEq employs the SIBYLL cosmic-ray interaction model^{58,59}, varied within systematic uncertainties as described elsewhere⁶⁰. Neutrinos from the decays of heavy hadrons are also incorporated, according to the BERSS model³⁵. The uncertainty deriving from the production height dependence is negligible for these energies. Uncertainties in the re-interaction cross section of kaons as they travel through the atmosphere are relevant and are included.

The astrophysical neutrino flux is simulated and propagated using parameters informed by existing IceCube measurements⁶¹, but with a wide systematic uncertainty on normalization and spectral index. The central model is taken to be a single unbroken power law in neutrino energy with a spectral index of 2.5. Variation in the astrophysical flux as a result of decoherence was tested and found to lead to negligible effects within the analysis sample. Each flux is propagated under the three-flavour oscillation formalism including decoherence, absorption and tau regeneration with the nuSQuIDS package³³ to provide an energy-, zenith- and flavour-dependent prediction at the detector for each oscillation hypothesis. The detector response to each flux is calculated by applying the reweighting protocol described in another work⁶² to a large Monte Carlo event ensemble to predict the final energy spectrum, which is used as an input to calculate the analysis likelihood test statistic.

All the systematic uncertainties are implemented as continuous nuisance parameters that are fitted through a profile log-likelihood analysis. The test statistic incorporates both accurate treatment of low-population bins and the effects of finite Monte Carlo sample size, and discussed elsewhere⁵⁶. The dominant sources of systematic uncertainty in this analysis are the detector performance uncertainties, which include the photon detection efficiency of the digital optical modules⁶³, the properties of the refrozen ice in the vicinity of the detector strings⁶⁴ and the properties of the bulk ice in the array⁶⁵. Depth-dependent uncertainties on optical absorption and scattering in the bulk glacial ice are accounted for as per the method described in another work 66. An improved ice model that incorporates crystal birefringence as a mechanism to explain the observed anisotropic light propagation in the glacier⁶⁷ was also tested within this analysis as a post-unblinding check, and was not observed to substantially affect the results.

Sub-leading systematic uncertainties associated with the primary cosmic-ray flux, evolution of atmospheric neutrino air showers, atmospheric density effects, astrophysical neutrino flux normalization and spectral shape, and neutrino cross section are also included. Extended Data Table 1 provides the full list of systematic uncertainties, their Gaussian priors and the best-fit values in one example decoherence scenario. Extended Data Fig. 1 shows the full distribution of pulls for each model point. The largest deviation on any systematic uncertainty is the cosmic-ray spectral index, which pulls to 2.3σ at its best-fit point. No other parameter deviates further than 1σ from the centre of its prior. This behaviour is qualitatively similar to what has been observed with previous IceCube analyses that have employed this sample to search for beyond-standard-model oscillation physics $^{53-55}$.

Data availability

A list of selected event energies and zenith angles, a Monte Carlo simulation set and information on systematic uncertainty effects, along with other public IceCube data releases, are available at https://icecube.wisc.edu/science/data-releases/.

Code availability

IceCube maintains an open-source repository of software tools for handling the IceCube data at https://github.com/IceCubeOpenSource. We also include scripts for handling the public data within the data release at https://icecube.wisc.edu/science/data-releases/.

References

- Ahn, E.-J., Engel, R., Gaisser, T. K., Lipari, P. & Stanev, T. Cosmic ray interaction event generator SIBYLL 2.1. Phys. Rev. D 80, 094003 (2009).
- Riehn, F., Engel, R., Fedynitch, A., Gaisser, T. K. & Stanev, T. Hadronic interaction model SIBYLL 2.3d and extensive air showers. *Phys. Rev. D* 102, 063002 (2020).
- Barr, G. D., Gaisser, T. K., Robbins, S. & Stanev, T. Uncertainties in atmospheric neutrino fluxes. *Phys. Rev. D* 74, 094009 (2006).
- Aartsen, M. G. et al. Characteristics of the diffuse astrophysical electron and tau neutrino flux with six years of IceCube high energy cascade data. *Phys. Rev. Lett.* 125, 121104 (2020).
- Abbasi, R. et al. LeptonInjector and LeptonWeighter: a neutrino event generator and weighter for neutrino observatories. Comput. Phys. Commun. 266, 108018 (2021).
- 63. Abbasi, R. et al. Calibration and characterization of the IceCube photomultiplier tube. *Nucl. Instrum. Methods Phys. Res., Sect. A* **618**, 139–152 (2010).
- Rongen, M. Measuring the optical properties of IceCube drill holes. EPJ Web Conf. 116, 06011 (2016).
- 65. Aartsen, M. G. et al. Measurement of South Pole ice transparency with the IceCube LED calibration system. *Nucl. Instrum. Methods Phys. Res., Sect. A* **711**, 73–89 (2013).
- Aartsen, M. G. et al. Efficient propagation of systematic uncertainties from calibration to analysis with the SnowStorm method in IceCube. JCAP 10, 048 (2019).
- 67. Abbasi, R. et al. In-situ estimation of ice crystal properties at the South Pole using LED calibration data from the IceCube Neutrino Observatory. *The Cryosphere* **18**, 75–102 (2024).

Acknowledgements

We acknowledge support from the following sources, grouped by country. United States: US National Science Foundation, Office of Polar Programs: US National Science Foundation, Physics Division: US National Science Foundation, EPSCoR: US National Science Foundation, Office of Advanced Cyberinfrastructure, Wisconsin Alumni Research Foundation, Center for High Throughput Computing (CHTC) at the University of Wisconsin-Madison; Open Science Grid (OSG), Partnership to Advance Throughput Computing (PATh), Advanced Cyberinfrastructure Coordination Ecosystem: Services & Support (ACCESS), Frontera computing project at the Texas Advanced Computing Center; US Department of Energy, National Energy Research Scientific Computing Center, Particle Astrophysics Research Computing Center at the University of Maryland; Institute for Cyber-Enabled Research at Michigan State University; Astroparticle Physics Computational Facility at Marquette University; NVIDIA Corporation; and Google Cloud Platform. Belgium: Funds for Scientific Research (FRS-FNRS and FWO), FWO Odysseus and Big Science programmes and Belgian Federal Science Policy Office (Belspo). Germany: Bundesministerium für Bildung und Forschung (BMBF), Deutsche Forschungsgemeinschaft (DFG), Helmholtz Alliance for Astroparticle Physics (HAP), Initiative and Networking Fund of the Helmholtz Association, Deutsches Elektronen Synchrotron (DESY), and High Performance Computing cluster of the RWTH Aachen. Sweden: Swedish Research Council, Swedish Polar Research Secretariat, Swedish National Infrastructure for Computing (SNIC) and Knut and Alice Wallenberg Foundation. European Union: EGI Advanced Computing for Research. Australia: Australian Research

Council. Canada: Natural Sciences and Engineering Research Council of Canada, Calcul Québec, Compute Ontario, Canada Foundation for Innovation, WestGrid and Digital Research Alliance of Canada. Denmark: Villum Fonden, Carlsberg Foundation and European Commission. New Zealand: Marsden Fund. Japan: Japan Society for Promotion of Science (JSPS) and Institute for Global Prominent Research (IGPR) of Chiba University. Korea: National Research Foundation of Korea (NRF). Switzerland: Swiss National Science Foundation (SNSF).

Author contributions

The IceCube Collaboration acknowledges significant contributions to this manuscript by the IceCube groups from the University of Texas at Arlington, the Niels Bohr Institute and Harvard University. The IceCube Collaboration designed, constructed and now operates the IceCube Neutrino Observatory. Data processing and calibration, Monte Carlo simulations of the detector and of the theoretical models,

and data analyses were performed by a large number of collaboration members, who also discussed and approved the scientific results presented here.

Competing interests

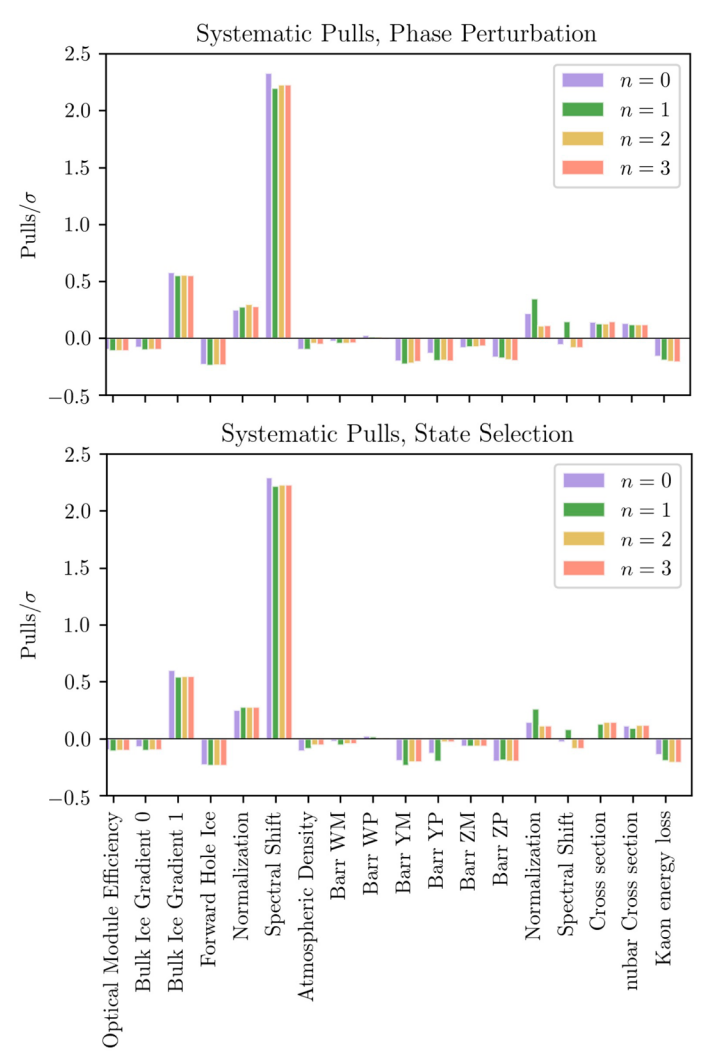
The authors declare no competing interests.

Additional information

Extended data is available for this paper at https://doi.org/10.1038/s41567-024-02436-w.

Peer review information *Nature Physics* thanks Ricardo A. Gomes, Atsuko Ichikawa and Giuseppe Gaetano Luciano for their contribution to the peer review of this work.

Reprints and permissions information is available at www.nature.com/reprints.



Extended Data Fig. 1 | **Systematic Pulls for Phase Perturbation (top) and State Selection (bottom).** The pull is defined as the value of the nuisance parameter minus its central value, divided by the Gaussian prior width. Each of the nuisance parameters (outlined in the Methods section) is represented by four color bars,

one corresponding to the best fit point under each power law n. Since the best fit point is very close to no decoherence in all power law models, the distributions of pulls are similar in all cases.

Extended Data Table 1 | Summary of nuisance parameters used in the analysis

		Value at Best Fit (n=0)		
Parameter	Prior	Phase	State	
		Perturbation	Selection	
Detector Parameters				
Optical Module Efficiency	0.97±0.10	0.96	0.96	
Bulk Ice Gradient 0	0.0±1.0*	-0.08	-0.07	
Bulk Ice Gradient 1	0.0±1.0*	0.58	0.60	
Forward Hole Ice (p ₂)	-1.0±10.0	-3.32	-3.30	
Conventional Flux Parameters				
Normalization(Φ_{conv})	1.0±0.4	1.10	1.10	
Spectral Shift ($\Delta_{conv.}$)	0.00±0.03	0.07	0.07	
Atmospheric Density	0.0±1.0	-0.10	-0.11	
Barr WM	0.00±0.40	-0.01	-0.00	
Barr WP	0.00±0.40	0.01	0.01	
Barr YM	0.00±0.30	-0.06	-0.06	
Barr YP	0.00±0.30	-0.04	-0.04	
Barr ZM	0.00±0.12	-0.01	-0.01	
Barr ZP	0.00±0.12	-0.02	-0.02	
Astrophysical Flux Parameters				
Normalization(Φ_{astro})	0.79±0.36*	0.84	0.84	
Spectral Shift ($\Delta_{astro.}$)	0.00±0.36*	-0.02	-0.01	
Cross sections				
Cross section $(\sigma_{ u_{\mu}})$	1.00±0.03	1.00	1.00	
Cross section ($\sigma_{\overline{ u}_{\mu}}$)	1.00±0.075	1.01	1.01	
Kaon re-interaction ($\sigma_{_{KA}}$)	0.0±1.0	-0.16	-0.14	

Each row specifies the constraint used in the frequentist analysis for each physics or nuisance parameter. All priors are one dimensional Gaussian functions, except in the case of the bulk ice and astrophysics flux parameters (marked with an asterisk) where a correlated prior is employed. The value of the nuisance parameters at best-fit point for n=0 are given for both state selection and phase perturbation interaction modes. A fully detailed description of these parameters and their technical implementations can be found in Ref. 52.